06,13

Influence of the upper electrode material on the electrophysical properties of MDM structures based on ferroelectric films

© M.S. Afanasyev, D.A. Belorusov, D.A. Kiselev, G.V. Chucheva ¶

Fryazino Branch, Kotel'nikov Institute of Radio Engineering and Electronics, Russian Academy of Sciences, Fryazino, Moscow oblast, Russia

¶ E-mail: gvc@ms.ire.rssi.ru

Received April 28, 2023
Revised April 28, 2023
Accepted May 4, 2023

Ferroelectric films of the composition $Ba_{0.8}Sr_{0.2}TiO_3$ (BST) were synthesized on platinized silicon substrates by RF sputtering. Top electrodes made of nickel, aluminum, copper and chromium were formed on the grown films by electron beam sputtering. The results of studies of the electrophysical properties of the obtained metal-dielectric-metal (MDM) heterostructures (Me-BST-Pt-Si) are presented.

Keywords: ferroelectric BST films, metal-dielectric-metal (MDM) structures, microstructure, electrophysical properties.

DOI: 10.21883/PSS.2023.06.56117.73

1. Introduction

Integration of ferroelectric materials with the modern microelectronic technologies and materials offers the opportunity of creating next generation devices and data storage devices based on nonlinear physical effects [1–3].

Layered perovskite composed of barium–strontium–titanium ($Ba_{0.8}Sr_{0.2}TiO_3$) is one of such promising ferroelectric materials. This compound is chosen as an active layer in a MIM-structure is associated with high permittivity near room temperature [4].

The objective of this study was to investigate the influence of the top electrode on electrophysical properties of MIM-structures based on $Ba_{0.8}Sr_{0.2}TiO_3$ ferroelectric films.

2. Samples and experimental methods

Platinized silicon wafers with adhesive titanium sublayer were used as substrates. $Ba_{0.8}Sr_{0.2}TiO_3$ (BST) ferroelectric films were formed by RF sputtering method. A ceramic target 50 mm in diameter with the equivalent composition was used for BST film deposition. The deposition chamber of the system was evacuated up to 10^{-3} Pa. Target sputtering was carried out in oxygen atmosphere at 10 Pa, discharge voltage $U = 450$ V, discharge current $I = 0.65$ A and evaporation rate 6 nm/s. After evaporation, all samples had a mirror surface.

Top electrodes were sputtered onto BST films through a shadow mask by electron beam vapor deposition at a deposition chamber residual pressure of 10^{-5} Pa, temperature of 70°C and evaporation rate of 2.0 Å/s. Electrode thickness was 100 ± 5 nm, area was $2.7 \cdot 10^{-4}$ cm^2. Electrode material: nickel (Ni), aluminium (Al), copper (Cu), chromium (Cr).

Thickness of BST films was measured by scanning electron microscopy (SEM) using FEI NovaNanoSem 230 microscope.

The structure of the produced BST films was investigated by the X-ray diffraction analysis method using DRON-3 automated double-crystal Bragg–Brentano diffractometer. A quartz monochromator and 0.15405 nm Cu $k\alpha_1$ emission were used.

BST film surface morphology, polarization switching processes were investigated using MFP-3D Stand Alone (Oxford Instruments Asylum Research, USA) scanning probe microscope. Residual piezoelectric hysteresis loops obtained in DART-PFM mode near the contact resonance of a „cantilever–film surface" system that was equal to ~ 0.9 MHz, then they were corrected using a simple harmonic oscillator [5,6]. Asyelec-02 (Oxford Instruments Asylum Research, USA) cantilevers were used to obtain hysteresis loops. AC voltage was 2 V. DC voltage varied in the range from -15 V to $+15$ V with step 0.75 V. DC voltage pulse supply time and piezoelectric response signal recording time after de-energizing were 12.5 ms.

Capacitance-voltage (C–V curve), frequency and temperature dependences of MIM-structures based on BST films were measured on an automated experimental setup [7] using LCR (Agilent) precision meter and Keithley picoammeter.

3. Results and discussion

3.1. Structural investigations of BST film structures

Figure 1 shows a BST film diffraction pattern.

The diffraction pattern contains peaks from different BST film planes that suggest the absence of prevailing orientation

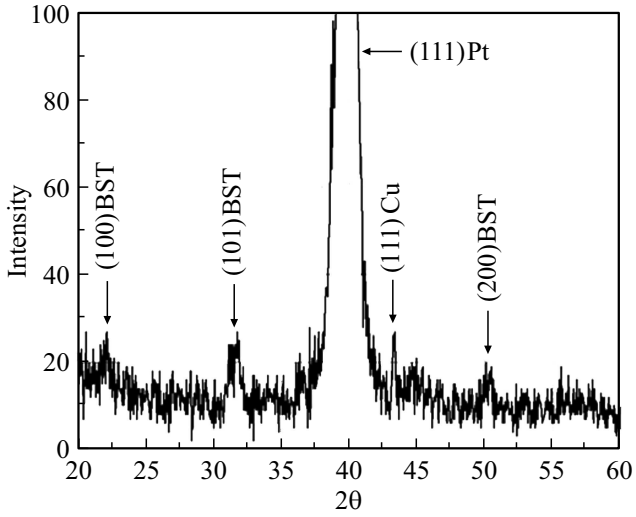

Figure 1. X-ray diffraction pattern of BST film.

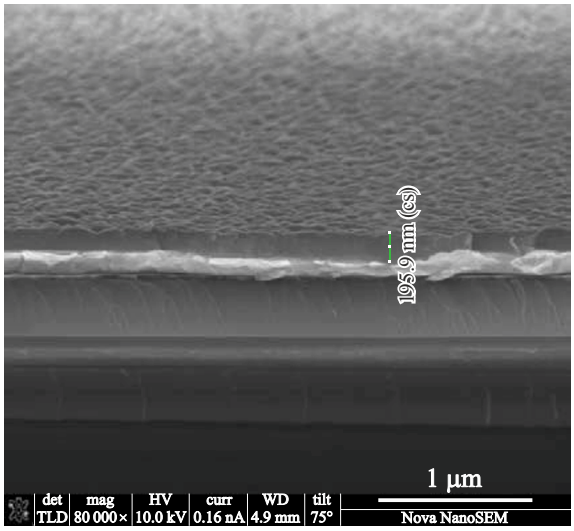

Figure 2. SEM image of a MIM-structure chip.

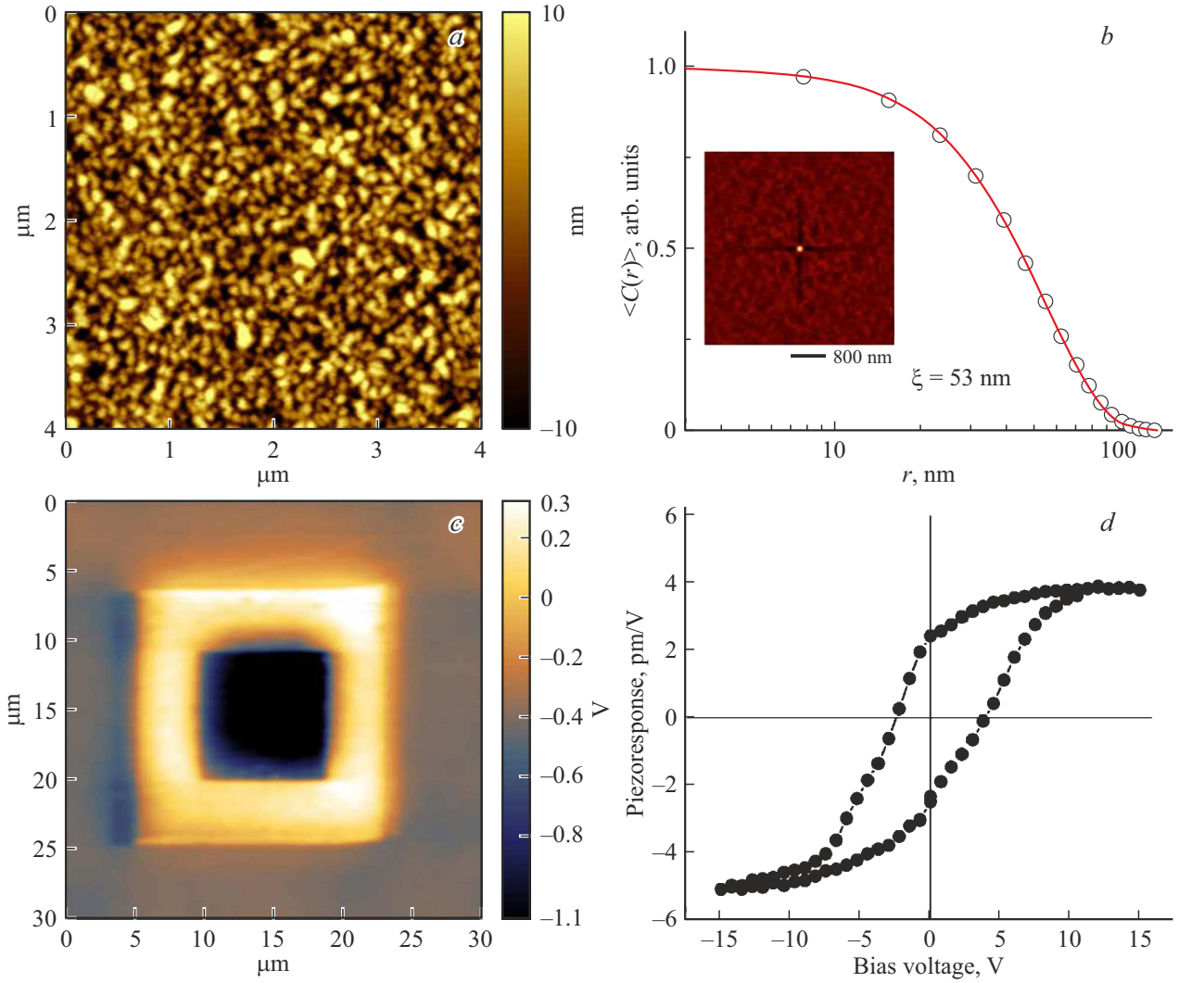

Figure 3. BST film surface image (*a*), diagram of radially averaged grain sizes (*b*) (detail — 2D representation of autocorrelation function), induced polarization image: light square — polarization at +8 V, dark square — polarization at −8 V (*c*), residual piezoelectric hysteresis loop (*d*).

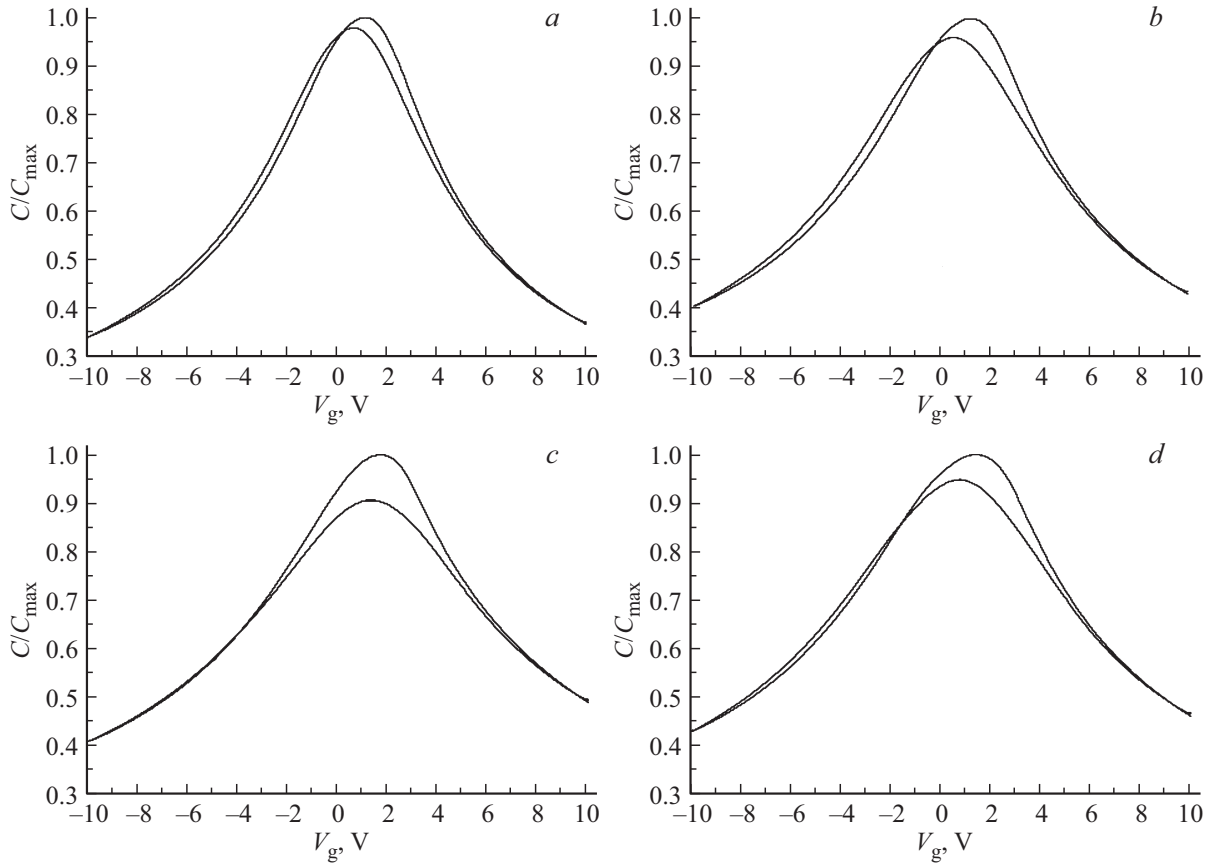

Figure 4. C–V curve of MIM-structures measured at room temperature and 1.0 MHz using various top electrodes: *a* — Ni, *b* — Cu, *c* — Al, *d* — Cr.

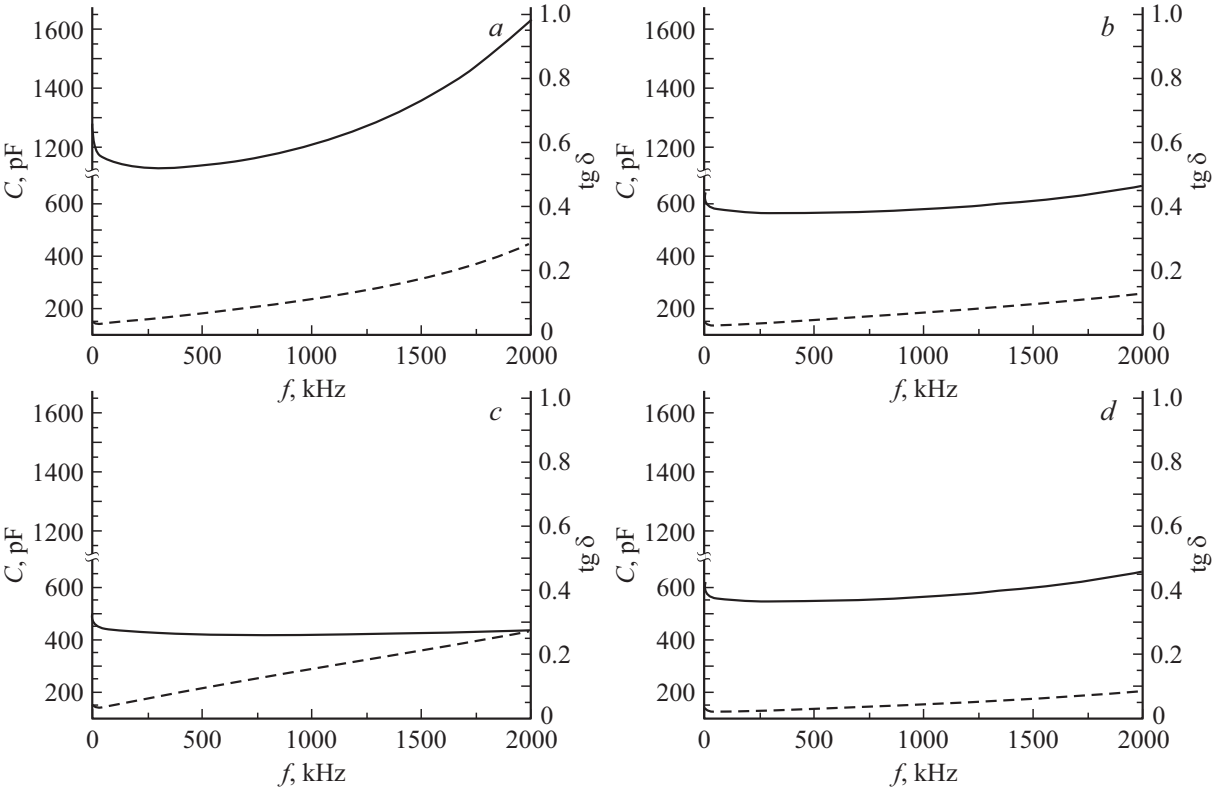

Figure 5. Dependence of capacity (solid line) and dielectric loss angle tangent (dashed line) of MIS structures on frequency: *a* — Ni, *b* — Cr, *c* — Al, *d* — Cu.

in the film. Angular position of peaks indicate stoichiometric composition of the film and the absence of macrostresses. Low intensity and considerable peak width suggest a low crystallite size.

Figure 2 shows SEM image of the MIM-structure recorded at 75°.

SEM image of the MIM-structure shows that the platinized layer thickness is 130 nm, BST film thickness is 200 ± 10 nm.

3.2. Investigations of BST film by scanning probe microscopy methods

Figure 3, *a* shows the BST film surface image, whose rms roughness (*Rms*) was equal to 5.1 nm. The presented scan image shows that the BST film is morphologically uniform, free of foreign contaminations and inclusions on the film surface. The average grain size was calculated using the autocorrelation function [8] in WSxM SPM image processing software [9]. Figure 3, *b* shows an approximated correlation function dependence for grain size averaging in the studied film. 2D image of the autocorrelation function obtained from the scanned surface image is shown in detail of Figure 3, *b*. The calculations have shown that the average grain size was 53 nm for the BST film synthesized on the platinized silicon substrate.

Piezoelectric properties of the thin BST film were investigated in piezoresponse force microscopy conditions. Figure 3, *c* shows an induced piezoresponse for the BST film after polarization at ± 8 VDC. Macrodomain regions were produced by film surface scanning with DC voltage applied to the conducting cantilever that served as a top electrode. Thus, the potential formed two polarized regions with an area of $20 \times 20\,\mu\text{m}^2$ („light region" — polarization at +8 V) and $10 \times 10\,\mu\text{m}^2$ („dark region" — polarization at −8 V).

In the polarization hopping spectroscopy mode, a residual piezoelectric hysteresis loop was obtained (Figure 3, *d*) that confirmed polarization hopping in a nanoscale region (within the cantilever-film surface contact area). hysteresis loop is asymmetric and characterized by low switching voltages: $V_{C+} = 3.9$ V and $V_{C-} = -2.4$ V. Such difference in voltages is associated with the presence of an internal displacement field induced by oxygen vacancies and spatial charge.

3.3. Electrophysical properties of MIM-structures

Figures 4 show C−V curves of MIM-structures with various top electrodes measures at room temperature and 1.0 MHz.

MIS structure capacity vs. displacement voltage curve is bell-shaped and shifted towards the positive region with respect to 0 V and has a loop formed by forward and reverse displacement voltage. Shift of maximum with respect to 0 V may be associated with the presence of internal electric field in the BST film which is induced by differences in the structures and charge states of the bottom and top Me/BST/Pt phase boundaries. Depending on the top electrode material, maximum capacity ($C_{\max}$) shift for Ni, Cu, Cr, Al was 1 V, 0.9 V, 1.1 V, 1.4 V, control coefficient of MIM-structures is 2.97, 2.52, 2.33, 2.44, respectively.

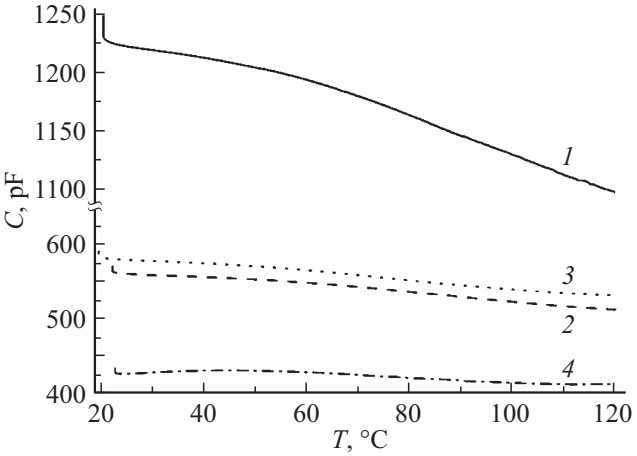

Figure 6. Dependence of the maximum capacity of MIS structures on temperature depending on the top electrode material: *1* — Ni, *2* — Cu, *3* — Cr, *4* — Al.

Figure 5 shows dependences of capacity (C) and dielectric loss angle tangent ($\tan\delta$) on frequency for MIM-structures measured at room temperature. The measurements were carried out at voltages corresponding to $C_{\max}$ on C−V curves of MIS structures.

For MIS structures with top Ni, Cu, Cr electrodes, capacity increase in the frequency range from 10 kHz to 2.0 MHz is typical. The maximum capacity increase is observed in MIM-structures with Ni from 1250 pF to 1600 pF. For MIS structure with Al, capacity remains unchanged.

The dielectric loss angle tangent ($\tan\delta$) was growing almost linearly and in the same way for all MIM-structures. The maximum increase in $\tan\delta$ was observed in a MIM-structure with Ni from 0.05 at 10 kHz to 0.27 at 2 MHz.

Figure 6 shows dependences of $C_{\max}$ on temperature for MIM-structures. The measurements were carried out in the temperature range from 20°C to 120°C at 1 MHz.

For the MIS structure with Ni, drop of $C_{\max}$ from 1230 pF at 20°C to 1100 pF at 120°C is observed, for other MIS structures with Cr, Al and Cu, $C_{\max}$ is almost unchanged.

4. Conclusion

X-ray diffraction measurements show stoichiometric composition of the BST film. According to the scanning probe microscopy, the average crystallite size is 53 nm. Possibility of local repolarization is shown based on the presence of induced polarized state and residual piezoelectric hysteresis loop. In addition, piezoresponse force microscopy of the test films shows residual polarization signal asymmetry

associated with the presence of internal field in the BST film.

The investigations have shown that the MIM-structure based on BST films have insignificant differences in electrophysical characteristics depending on the top electrode material. The temperature investigations have shown that the MIM-structures with top Cr, Al and Cu electrodes are rather thermally stable within the temperature range from 20 to 120°C and have their capacity varied by not more than 10%.

The investigations show that Cr, Al and Cu are the most suitable materials for electrodes in MIM-structures based on BST films.

Funding

This study was supported by grant No. 22-19-00493 provided by the Russian Science Foundation (https://rscf.ru/project/22-19-00493/.).

Conflict of interest

The authors declare that they have no conflict of interest.

References

[1] D.A. Abdullaev, R.A. Milovanov, R.L. Volkov, N.I. Borgardt, A.N. Lantsev, K.A. Vorotilov, A.S. Sigov. Russ. Technol. J. **8**, *5*, 44 (2020).
[2] K.A. Vorotilov, V.M. Mukhortov, A.S. Sigov. Integrirovannye segnetoelektricheskie ustroystva. Energoatomizdat, M., (2011). 175 p. (in Russian).
[3] K.M. Rabe, Ch.G. An, Zh.-M. Triskon. Fizika segnetoelektrikov: sovremennyi vzglyad. Laboratoriya znanij, Gorod (2020). 443 p. (in Russian).
[4] V.M. Mukhortov, Yu.I. Yuzyuk. Geterostruktury na osnove nanorazmernykh segnetoelektricheskikh plyonok: poluchenie, svoistva i primenenie. YuNTs RAN, Rostov n/D (2008), 221 p. (in Russian).
[5] A. Gannepalli, D.G. Yablon, A.H. Tsou, R. Proksch. Nanotechnology **24**, 159501 (2013).
[6] J. Bian, P. Xue, R. Zhu, L. Wang, B. Yang, T. Li, Q. Hu, L. Shen, J. Wang, G. Lu, Y. Yang. Appl. Mater. Today **21**, 100789 (2020).
[7] E.I. Goldman, A.G. Zhdan, G.V. Chucheva. PTE **6**, 110 (1997). (in Russian).
[8] M.S. Afanasyev, D.A. Kiselev, S.A. Levashov, A.A. Sivov, G.V. Chucheva. FTT **61**, *10*, 1948 (2019). (in Russian).
[9] R.C. Munoz, G. Vidal, M. Mulsow, J.G. Lisoni, C. Arenas, A. Concha, R. Esparza. Phys. Rev. B **62**, *7*, 4686 (2000).